C22

Intracellular calcium dynamics alters the membrane stability of a virtual ventricular mid-myocardial cell

W. Tong and A.V. Holden

Institute of Membrane and Systems Biology, University of Leeds, Leeds, UK

We aimed to evaluate the relative role of membrane and $[Ca^{2+}]_i$ dynamics in the formation of early afterdepolarisations (EADs). We analysed the membrane system (i.e. with all intra- and extra-cellular ionic concentrations clamped) of a Luo-Rudy ventricular cell model (LRd00; [1]) using continuation algorithms with the maximal conductance of the slow delayed rectifying K^+ current (g^*_{Ks}) as the bifurcation parameter (Fig. 1a).

A stable equilibrium existed at membrane potential V ≈ -88.5 mV for all g^*_{Ks}. Unstable oscillations states (OS) were found in between $0.105 < g^*_{Ks} < 0.223$ mS μF^{-1}, within the physiological range. These OS originated from a subcritical Hopf bifurcation (HB) at $g^*_{Ks} \approx 0.18$ mS μF^{-1}. Two equilibria coexisted (bistability) for g^*_{Ks} below the HB. The g^*_{Ks} of a LRd00 epi-: mid-: endocardial cells are 0.433: 0.125: 0.289 mS μF^{-1} [2]. The LRd00 mid-myocardial membrane model is bistable, whereas the epicardial and endocardial membrane models have a single stable equilibrium. This is confirmed by numerical integration from different initial conditions (Fig. 1b). The addition of $[Ca^{2+}]_i$ dynamics to the mid-myocardial membrane restored the model to a single equilibrium (Fig. 1d). Action potentials and EADs in the cell model (Fig. 1c) showed similar plateau and repolarization dynamics as the transients in Fig. 1d.

$[Ca^{2+}]_i$ dynamics prevents the bistability of the mid-myocardial membrane model, and accounts for the EAD family of waveforms.

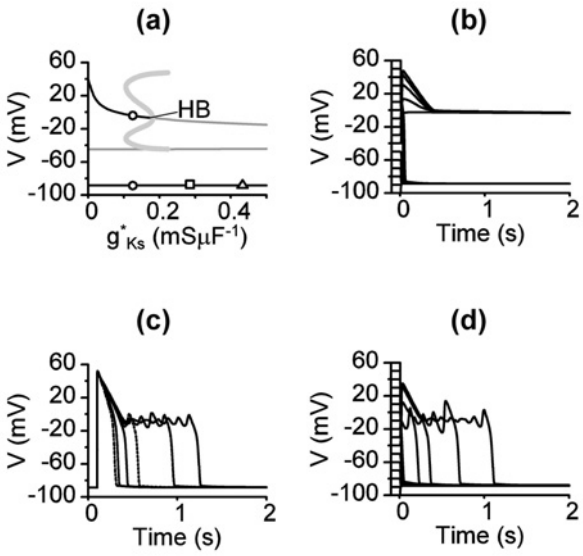

Figure 1. (a) Bifurcation diagram of the membrane system (LRd00, clamped ionic concentrations) for g^*_{Ks} shows the membrane potential (V) at which $dV/dt = 0$: stable equilibria (black line), unstable equilibria (grey line), unstable periodic (grey circles) and Hopf bifurcation (HB). Stable equilibria for epicardial (triangle), mid-myocardial (black circles) and endocardial membrane (square) are indicated. (b) For the mid-myocardial membrane, after 2 s at holding V, $V(t)$ converge into two stable equilibria but (d) addition of $[Ca^{2+}]_i$ dynamics with the mid-myocardial membrane leaves one stable equilibrium. (c) Overlay of solitary action potentials in a simulated LRd00 cell with $[Ca^{2+}]_i$ dynamics and g^*_{Ks}, decreased from left to right: 0.433, 0.289, 0.163, 0.150, 0.137, 0.125 mS μF^{-1}, show prolonged action potential duration with EADs.

Faber GM & Rudy Y (2000). Biophys J **78**, 2392-2404.

Viswanathana PC *et al.* (1999). Circulation **99**, 2466-2474.

This work was supported by the European Union through the Network of Excellence BioSim, Contract No. LHSB-CT-2004-005137. W.C.T. is supported by a British Heart Foundation research studentship (FS/03/075/15914).

Where applicable, the authors confirm that the experiments described here conform with the Physiological Society ethical requirements.

C23

Human ventricular fibrillation: mother rotor or multiple wavelets?

A. Mourad[1], M.P. Nash[1], R.H. Clayton[2], C.P. Bradley[3], P.M. Sutton[4], M. Hayward[4], D.J. Paterson[3] and P. Taggart[4]

[1]Bioengineering Institute, University of Auckland, Auckland, New Zealand, [2]Department of Computer Science, University of Sheffield, Sheffield, UK, [3]Department of Physiology, Anatomy & Genetics, University of Oxford, Oxford, UK and [4]Departments of Cardiology and Cardiothoracic Surgery, University College London Hospitals, London, UK

Mechanisms underpinning ventricular fibrillation (VF) are poorly understood. Maintenance of VF by a single re-entrant

source (mother rotor) or by multiple wavelets have both been implicated. We aimed to characterise the spatiotemporal dynamics of early VF in humans using total epicardial electrical mapping.

In 10 patients undergoing cardiac surgery, VF was induced by burst pacing, and a 20-40 s episode of fibrillatory activity was sampled at 1 kHz using an epicardial sock containing 256 unipolar contact electrodes connected to a UnEmap system. Dominant frequencies (DF) were computed for each electrode signal using the fast Fourier transform [1]. We also transformed voltage into phase using the Hilbert transform. Phase singularities (PS) [2] and activation wavefronts (WF) [3] were identified and quantified.

Regression analysis showed a small but significant increase in the mean DF at a rate of 0.018±0.005 Hz/s ($p<0.01$) during early VF across all electrodes of all hearts. Moreover, large wavefronts with significant organisation were present for the majority of VF recordings. Each patient had a median number of PS between 4 and 9, and a median number of WF between 3 and 7, indicative that early VF is driven by a small number of electrical sources. Our recordings demonstrated multiple electrophysiological activation patterns. For example, in the fibrillating heart of one patient, we observed (i) persistent clockwise rotation of a single epicardial re-entrant wave; (ii) persistent anti-clockwise epicardial re-entry (Fig. 1, left); and (iii) epicardial breakthrough patterns. Moreover, these organised patterns were punctuated by: (iv) disorganised wave activity with many interacting re-entrant sources (Fig. 1, right). Throughout the entire VF episode, the electrophysiological activity continually switched between these organised and disorganised behaviours. This type of transitional VF activity was observed for all patients.

We found that early human VF was typically sustained by a small number of re-entrant sources that were associated with large and coherent WF (mother rotors). However, at times we also observed a large number of small WF (multiple wavelets). Thus, our results suggest that multiple electrophysiological mechanisms sustain VF in the human heart.

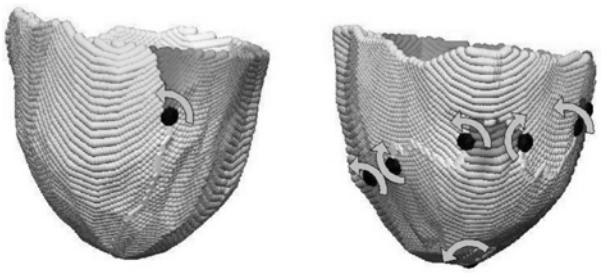

Figure 1. A single epicardial re-entrant wave (left), and multiple epicardial wavefronts (right) in the same patient. The spectrum shows electrophysiological phase, and filled circles show phase singularities (with chirality indicated by the arrows) at the ends of the wavefronts (grey lines).

Zaitsev AV, Berenfeld O, Mironov SF, Jalife J & Pertsov AM (2000). Circ Res 86, 408-417.

Bray M-A & Wikswo JP (2002). IEEE Trans Biomed Eng 49, 1086-1093.

Rogers JM (2004). IEEE Trans Biomed Eng 51, 56-65.

Where applicable, the authors confirm that the experiments described here conform with the Physiological Society ethical requirements.

C24

A pore region novel SCN5A mutation (R878C) associated with sick sinus syndrome and Brugada syndrome ECG in a Chinese family

Y. Zhang[1], A. Ma[1], H. Wan[1], M. Lei[2], X. Zhou[1], C. Huang[1] and R. Shi[1]

[1]Cardiology, Xi'an Jiaotong University, Xi'an, Shaanxi Province, China and [2]Division of Cardiovascular and Endocrine Sciences, School of Medicine, Manchester, UK

Sick sinus syndrome (SSS) refers to an arrhythmic phenotype attributed to sinus node dysfunction manifesting as sinus bradycardia, sinus arrest and/or sinoatrial block. Recently Benson et al. (2003) reported that heterozygous mutations of SCN5A, the gene that encodes for the alpha subunit of the cardiac sodium channel, caused congenital SSS characterized as an autosomal recessive disorder of this channel.

Here we report a novel mutation (R878C) of SCN5A associated with SSS in a Chinese family. In contrast to Benson et al. (2003), the transmission of the phenotype of this mutation is autosomal dominant with reduced penetrance in this family. Based on associations with disorders of cardiac rhythm and conduction, we screened SCN5A as a candidate gene in three generations of this Chinese family. Four individuals from this family exhibit a heterozygosic mutation C to T transition at nucleotide 2826 (Gen-Bank accession number: DQ086162), encoding cysteine in place of arginine 878 (designated as R878C). This novel mutation is located in the linker between S5 and S6 of Domain II (DII), a region which forms the pore of the Nav1.5 channel. Two mutation carriers are SSS patients, one carrier has a Brugada syndrome-like ECG and one carrier is clinical normal. Interestingly, three other mutations (F892I, C896S and S901L; Priori et al. 2002) were also identified in the pore region between S5 and S6 in the DII in this channel. All these mutations are associated with Brugada syndrome and are loss-of-function mutations. Therefore, it is likely that this region plays a crucial role for maintaining normal function of the cardiac sodium channel. Further biophysical characterization of this novel mutation is being conducted in the mammalian cell expression system.

Benson DW, Wang DW, Dyment M et al. (2003). J Clin Invest 112, 1019-1028.

Priori SG, Napolitano C, Gasparini M et al. (2002). Circulation 105, 1342–1347.

This work is supported by National Nature Sciences Foundation of China (No. 30371571), and International Cooperation Projects of the Ministry of Science and Technology of China (2003DF000037).

Where applicable, the authors confirm that the experiments described here conform with the Physiological Society ethical requirements.

C25

Quantitative microstructure of rat right-ventricular trabeculae carnae

P. Joshi[2], G. Sands[1], D. Gerneke[1], I. LeGrice[2] and D. Loiselle[2]

[1]*Bioengineering Institute, The University of Auckland, Auckland, New Zealand and* [2]*Department of Physiology, School of Medical and Health Sciences, The University of Auckland, Auckland, New Zealand*

Due to their small diameter and the axial alignment of their myocytes, isolated trabeculae carnae are extensively used in studies of the mechanics of cardiac tissue. An understanding of their structure is essential for the interpretation of results arising from such studies. Our aim was to quantify the relative proportions of myocytes, connective tissue and blood vessels constituting right-ventricular trabeculae carnae from adult rats.

Isolated hearts were Langendorff-perfusion fixed with 3% formalin in high osmolarity phosphate buffer. A trabecula was dissected from the ventricular free wall and embedded in a resin block. The block was fixed onto the translation stage of an extended-volume imaging system (1) and its surface milled to expose the preparation in cross-section. The exposed surface was etched (2), stained with toluidine blue (for myocytes), followed by ponceau de xylidine and acid fuchsin (for connective tissue), and photographed using a digital camera attached to a compound light microscope with a 20x, 0.7 NA, water-immersion lens. The samples were milled at 20 μm intervals to obtain a series of sequential cross-sectional images.

In order to calculate fractional areas, images were segmented, based upon colour and intensity differences. The relative areas (mean ± 95% confidence limits, n = 8) were: 0.77 ± 0.028 myocytes, 0.11 ± 0.030 collagen and 0.11 ± 0.018 blood vessels. With the exception of those in the peripheral layer, essentially every myocyte had at least one immediately adjacent capillary while, on average, each capillary serviced two myocytes. Three-dimensional reconstruction (at 1 μm intervals) of a 50 μm segment revealed that most axially-aligned capillaries are interconnected, at some point, forming a reticulated microvascular network within the trabecula.

Sands G, Gerneke D, Hooks DA, Green CR, Smaill BH & LeGrice IJ (2005). Microscopy Research and Techniques 67, 227-239.

Maxwell M (1978). J Microsc 112, 253-255.

The study was supported by the National Heart Foundation of New Zealand.

Where applicable, the authors confirm that the experiments described here conform with the Physiological Society ethical requirements.

C51

Voluntary exercise-induced changes to β1- and β2-adrenergic receptor stimulation in rat left ventricular myocytes

R. Stones, R. Billeter, S. Harrison and E. White

Institute of Membrane and Systems Biology, The University of Leeds, Leeds, UK

During exercise there is an increase in the circulating levels of catecholamines and enhanced sympathetic tone (Scheurink *et al.* 1989). As a result, several studies have documented beta-adrenergic receptor (β-AR) modification which may represent one of the mechanisms underlying the relative bradycardia in trained subjects (Werle *et al.* 1990). In light of this, we investigated whether the response of β-AR to stimulation was altered in a model of voluntary wheel running exercise in female rats (Natali *et al.* 2002).

Following 6-7 weeks of voluntary running, heart weight: body weight was significantly greater in trained (TRN) than sedentary (SED) animals (5.6 ± 0.1 *vs* 4.8 ± 0.1, TRN *vs* SED, respectively, (mean ± SEM, $P<0.001$, unpaired t test, n = 24 in each group). Left ventricular myocytes were isolated from the hearts of TRN and SED rats and field stimulated to evoke contraction at a frequency of 1 Hz at 37°C. Contraction magnitude was measured optically and was expressed as a percentage of resting cell length.

Selective β1-AR stimulation (isoprenaline, 10^{-7} M, in the presence of the β2-AR antagonist, ICI 118,551, 10^{-7} M) was unaltered by exercise but the inotropic response to β2-AR stimulation (salbutamol, $5x10^{-5}$ M, in the presence of β1-AR blockade, atenolol 10^{-7} M) was significantly depressed in TRN cells (50.0 ± 6.8 *vs* 18.5 ± 8.0%, SED *vs* TRN, respectively, $P < 0.05$, unpaired t test, n = 47-54 cells). β2-AR stimulation activates both G_i and G_s signalling cascades. To investigate whether the reduced response to β2-AR stimulation in the TRN myocytes was a result of enhanced G_i signalling, left-ventricular myocytes were incubated in pertussis toxin (PTX, 2-3 hrs at 37°C) to inhibit G_i protein function. The contractile response to β2-AR stimulation was enhanced in both TRN and SED groups following PTX pretreatment to a similar level, i.e. the depressive effect of exercise on the inotropic response to β2-AR was abolished by PTX (72.6 ± 10.5 *vs* 68.6 ± 9.8%, SED *vs.* TRN, respectively, NS, n= 31 – 32 cells).

We conclude that voluntary exercise training induces a decrease in the positive inotropic response to β2-AR stimulation and this is at least in part due to enhanced G_i signalling. These effects contrast with the depression in β1-AR responsiveness with maintained β2 responsiveness reported in failing myocardium.

Scheurink AJW *et al.* (1989). *Am J Physiol Regulatory Integrative Comp Physiol* **256**, R155-R160.

Werle EO *et al.* (1990). *Life Sci* **46**, 9-17.

Natali AJ *et al.* (2002). *J Physiol* **541**, 863-875.

Funded by the British Heart Foundation.

Where applicable, the authors confirm that the experiments described here conform with the Physiological Society ethical requirements.

C52

Stretch-activated channels contribute to the length-dependent slow force response of isolated mouse myocardium

M. Ward[1] and D.G. Allen[2]

[1]*Physiology, University of Auckland, Auckland, New Zealand and* [2]*Institute for Biomedical Research, University of Sydney, Sydney, NSW, Australia*

When cardiac muscle is subjected to stretch the force of contraction increases, allowing the intact heart to adjust its output to the body's demand (Allen & Kentish, 1985). This increase in contractility has been shown in vivo to occur in two distinct phases. Initially there is an abrupt increase in force that coincides with the stretch, and secondly there is a slower response that develops over a period of a few minutes (the 'slow force response'). The first of these responses is largely due to a change in the sensitivity of the contractile proteins to Ca^{2+}, whereas the slow force response is accompanied by a concomitant increase in the magnitude of the intracellular Ca^{2+} transient (the event that initiates contraction). It has been proposed that stretch-activated channels contribute to Ca^{2+} entry after stretch (Calaghan & White, 2004). The aim of the present study was to reinvestigate the mechanisms underlying the slow force response of cardiac muscle.

Mice (C57 BL10) were killed by intraperitoneal injection of 100 mg/kg body wt sodium pentobarbitone, mixed with 10 mg/kg body wt heparin to prevent blood coagulation, and hearts rapidly removed. Cardiac trabeculae, or small diameter papillary muscles (< 1 mm in length, and 0.1-0.3 mm in diameter), were dissected from the right ventricle, and mounted in a muscle chamber between a hook attached to a force transducer and a lever connected to a motor capable of making precise changes in muscle length. Each preparation was then subjected to a step increase in length for 2 min whilst isometric force was recorded. One minute after the initial length change active force increased by 77 ± 17% of the force immediately following the stretch (n = 16). Subsequent application of either 400 μM streptomycin, or 20 μM $GdCl_3$ (blockers of stretch-activated channels) reduced the slow force response ($p \leq 0.01$, paired t-test) for identical step increases in length (streptomycin: from 86 ± 25% to 38 ± 14% (n=9), or $GdCl_3$: from 65 ± 21% to 12 ± 7%, n=7), suggesting a possible role for stretch-activated channels in the slow force response. The involvement of these channels was further tested by incubating preparations with 10 μM GsMTx-4, a specific blocker of stretch-activated channels (Suchyna et al. 2000). In the presence of GsMTx-4 the slow force response 1 min following the stretch was reduced from 112 ± 40% in the absence of the toxin, to 15 ± 8% (n=6, $p \leq 0.01$ Mann-Whitney Rank Sum test). These results confirm a role for stretch-activated channels in the slow force response of mouse myocardium.

Allen DG & Kentish JC (1985). J Mol Cell Cardiol 17, 821-840.

Calaghan S & White E (2004). J Physiol 559, 205-214.

Suchyna TM, Johnson JH, Hamer K, Leykam JF, Gage DA, Clemo HF, Baumgarten CM & Sachs F (2000). J Gen Physiol 115, 583-598.

Where applicable, the authors confirm that the experiments described here conform with the Physiological Society ethical requirements.

C53

Uncaging acid in ventricular myocytes using UV flash photolysis of 2-nitrobenzaldehyde

P. Swietach[1], K.W. Spitzer[2] and R.D. Vaughan-Jones[1]

[1]Burdon Sanderson Cardiac Science Centre, Oxford University, Oxford, UK and [2]Nora Eccles Harrison Cardiovascular Research and Training Institute, University of Utah, Salt Lake City, UT, USA

The membrane-permeant caged-H^+ substance, 2-nitrobenzaldehyde (NBA), undergoes intramolecular redox catalysed by UV light. The product of photolysis is a strong acid, 2-nitrosobenzoic acid (pK=2.2), which is trapped intracellularly and which releases H^+. Rat ventricular myocytes, AM-loaded with the pH-sensitive dye, carboxy-SNARF-1, were superfused (37°C) with Hepes-buffered Tyrode solution containing 1mM NBA and 30μM cariporide (to inhibit Na^+-H^+ exchange). In the absence of UV light, NBA itself had no effect on resting pH, cell contraction or evoked Ca^{2+} transients. Myocytes were imaged confocally (Leica TCS NT) while excitation was provided alternately by an Argon laser (514nm) to image intracellular pH (pH_i) and by a UV laser (351nm, 20mW) to flash-photolyse NBA. At 100% UV laser power, the quantum yield of NBA photolysis reaches 65% (pixel dwell time <10μs). The magnitude and area of H^+ release can be controlled through neutral density filters and by limiting the scanning window, respectively. Exposing a small region (typically 4x4μm) of a cell to repetitive (0.11Hz) flashes of UV light, interrupted by a period of pH_i data acquisition, produces a local cumulative rise in $[H^+]$ that dissipates by diffusion. The time-course of $[H^+]$ rise in selected regions of a single myocyte can be used to measure the apparent H^+ diffusion coefficient (D_H^{app}), estimated as $13.4\pm1.6\times10^{-7}$ cm^2/s (n=46) using diffusion equations. This technique was also applied to cell-pairs to measure the apparent junctional H^+ permeability constant (P_H^{app}). The time-course of $[H^+]$ rise in side-by-side and end-to-end myocyte pairs gave an estimate for P_H^{app} of $0.35\pm0.05\times10^{-4}$ cm/s (n=21) and $3.6\pm1.1\times10^{-4}$ cm/s (n=7), respectively (significant anisotropy of permeation). Replacing Hepes with 5% CO_2/bicarbonate in the superfusion solutions increases D_H^{app} and P_H^{app} by ~30-40%. This is consistent with the role of CO_2/bicarbonate, an open buffer, in facilitating intracellular H^+ mobility. The present technique may also be useful for studying the spread of acidosis within multicellular cardiac preparations, including localised regions of the whole-heart, and in studying the spatial interactions between pH and other signalling molecules such as Ca^{2+}.

This work is supported by the British Heart Foundation (UK) and National Institutes of Health (USA).

Where applicable, the authors confirm that the experiments described here conform with the Physiological Society ethical requirements.

C54

Disruption of caveolae converts 'local' β_2 adrenoceptor signalling to a more diffuse global signal in the rat ventricular myocyte

S. Calaghan

Institute of Membrane and Systems Biology, University of Leeds, Leeds, UK

β_1 adrenoceptors (ARs) couple to G_s proteins whereas β_2 ARs couple to both G_s and G_i. It is G_i protein activation that confines the cAMP-dependent β_2 AR signal to the membrane compartment (Chen-Izu et al. 2000). We have recently shown that disrupting caveolae (invaginated lipid raft domains) in rat ventricular myocytes enhances the inotropic response to β_2 AR stimulation, and that this effect can be mimicked by disabling G_i signalling with pertussis toxin (Calaghan & White, 2006). If G_i signalling requires caveolae, disrupting caveolae should convert the membrane-localised β_2 signal to a more diffuse signal that reaches intracellular targets such as the sarcoplasmic reticulum and the myofilaments. This hypothesis has been tested by looking at the effect of caveolar disruption on the phosphorylation of phospholamban (PLB) and one of its functional correlates (the rate of relaxation) in response to β_2 AR stimulation.

Rat ventricular myocytes were treated with methyl-β-cyclodextrin (MβC) to disrupt caveolae (see Calaghan & White, 2006). β_2 AR stimulation was achieved with 50 μM salbutamol in the presence of 1 μM atenolol. All myocytes were field-stimulated (0.5 Hz) and maintained at room temperature (22-24°C). Populations of cells were fixed under basal conditions, or at 5 min after β_2 AR stimulation. Phosphorylation of PLB was measured following SDS-PAGE and Western blotting using an antibody specific for Ser^{16}-phosphorylated PLB (Calaghan et al., 1998). Change in phosphorylation status was assessed with densitometry. Some cells were perfused with salbutamol and atenolol through a rapid-switching device and the lusitropic response indexed by $t_{0.5}$ relaxation at steady state (≈5 min).

A reduction in $t_{0.5}$ relaxation in response to β_2 AR was observed in both populations of cells, but the effect was much greater ($P<0.05$; Student's *t* test) in myocytes in which caveolae were disrupted (-25.9 ± 5.1%; mean ± S.E.M; n=19 cells) than in controls (-13.8 ± 2.9%; n=19). Preliminary data showed a 42.6 ± 10.5% increase in phosphorylation of PLB at Ser^{16} in response to β_2 AR stimulation in MβC-treated cells which bordered on significance ($P=0.056$; n=3 hearts; *t* test). However, no change in Ser^{16}-phosphorylated PLB was seen following β_2 AR stimulation in controls ($P>0.2$; n=3).

These data suggest that disruption of caveolae in the adult ventricular myocyte converts the more membrane-confined β_2 AR cAMP-dependent signal to a global β_1-like response, and provide further support for the hypothesis that coupling of G_i proteins to the β_2 AR receptor requires the spatial confinement offered by caveolae.

Chen-Izu Y et al. (2000). *Biophys J* **79**, 2547-2556.

Calaghan SC & White E (2006). *Cardiovasc Res* **69**, 816-824.

Calaghan SC et al. (1998). *Pflugers Arch* **436**, 948-956.

This work was sponsored by the British Heart Foundation.

Where applicable, the authors confirm that the experiments described here conform with the Physiological Society ethical requirements.

PC89

Rhythm disturbances in the streptozotocin-induced diabetic rat heart

F.C. Howarth[1], M.A. Qureshi[1] and M. Lei[2]

[1]Physiology, United Arab Emirates University, Al Ain, Abu Dhabi, United Arab Emirates and [2]Cardiovascular & Endocrine Sciences, Unversity of Manchester, Manchester, UK

Previous in vivo biotelemetry studies have demonstrated reductions in heart rate and heart rate variability in the strepozotocin (STZ)–induced diabetic rat (Howarth et al. 2005). These heart rhythm disturbances may be attributed to extrinsic defects in autonomic control and/or intrinsic defects in the conduction system of the heart. We have investigated the effects of STZ–induced diabetes on intrinsic heart rhythm. Diabetes was induced by a single intraperitoneal injection of STZ (60 mg/kg) administered to young male Wistar rats (200-250g). Experiments were performed 8-10 weeks after STZ treatment. In some experiments spontaneous heart rates were recorded in Langendorf perfused (8 ml/g heart/min) hearts perfused with a normal Tyrode solution containing 1.8 mM Ca^{2+} maintained at 35-37°C. In other experiments an isolated sinoatrial node (SAN) preparation containing the SAN and part of the right atrium was dissected. The preparation was then placed in a tissue bath and superfused at 4 ml/min with normal Tyrode solution at 35±0.5°C. Extracellular potentials (ECPs) were recorded by two bipolar electrodes from the isolated SAN preparations as described by Lei et al. (2004). Electrodes were placed in the centre of the sinoatrial node and in the neighbouring atrial muscle in the right atrial appendage. Data are expressed as means ± S.E.M. (with number of preparations). Statistical comparisons were made with Independent samples t test with a P value of <0.05 considered significant. Diabetes was confirmed by a significant elevation of blood glucose (365±33 mg/dl, n=7) compared to age-matched controls (66±4 mg/dl, n=7) and a reduced body weight gain in diabetic rats (235±9 g, n=7) compared to controls (352±9 g, n=7). Heart rate recorded in Langendorff perfused hearts was significantly lower in diabetic rats 171±12 bpm (n=6) compared to 229±9 bpm (n=6) in controls. The pacemaker cycle length and the sino-atrial conduction time were significantly prolonged in diabetic SAN preparations (415.2±42.6 and 12.3±1.8 ms, n=6) compared to controls (255.2±6.7 and 7.4±0.6 ms, n=6). Heart rhythm defects in the STZ-induced diabetic rat might be partly attributed to intrinsic defects in sinus rhythm generation and conduction between the SAN and neighbouring atrium.

Howarth FC, Jacobson M, Naseer O, Adeghate E (2005). Exp Physiol 90, 237-245.

Lei M, Jones SA, Liu J, Lancaster MK, Fung SS, Dobrzynski H et al. (2004). J Physiol 559, 835-848.

Work supported by the British Council and the Wellcome Trust.

Where applicable, the authors confirm that the experiments described here conform with the Physiological Society ethical requirements.

PC90

Interaction of Ca^{2+}-calmodulin protein kinase II delta (CaMKIIδ) with sorcin

D. Anthony and S. Currie

Dept of Physiology and Pharmacology, University of Strathclyde, Glasgow, UK

CaMKIIδ has been shown to modulate cardiac sarcoplasmic reticulum (SR) Ca^{2+} release via interaction with the ryanodine receptor (RyR2) complex [1]. However, the nature and functional consequences of this interaction remain unclear. CaMKIIδ may interact directly with RyR2 or with accessory proteins that exist as part of the multi-protein channel complex. In this study, we have explored the possibility that CaMKIIδ may interact directly with sorcin and that RyR2 may be modulated via this route. Sorcin is a 22kDa member of the penta EF-hand family of Ca^{2+} binding proteins. It has been shown to negatively modulate RyR2 channel open probability and this is dependent on the phosphorylation status of sorcin [2].

We have examined the possibility of direct CaMKIIδ-sorcin interaction in surface plasmon resonance (SPR) studies, which allow direct protein-protein interactions to be measured in real time. One protein is immobilised on a sensorchip while the other is injected over the chip surface. Protein binding is measured by a change in refractive index expressed as response units (RU). We used recombinant sorcin and $CaMKII\delta_C$ in SPR experiments. The $CaMKII\delta_C$ isoform variant was used since this is the isoform expressed in the cytosol of cardiomyocytes and is involved in regulation of excitation-contraction coupling [3]. Conditions were optimised for $CaMKII\delta_C$ immobilisation. Sorcin (0.3-1μM) and calmodulin (0.3-1μM) were used as analytes. We then explored the nature of the sorcin-CaMKIIδ interaction in more detail by (i) measuring kinase activity in the presence and absence of sorcin and (ii) examining if sorcin may be a substrate for CaMKIIδ.

SPR studies suggest that CaMKIIδ and sorcin interact. The CaMKIIδ-sorcin interaction is weaker (10.85±2.05 RU) than the CaMKIIδ-calmodulin interaction (52.98±3.13 RU) (n=4, P=0.00003). It can occur in the presence or absence of calmodulin and is Ca^{2+} dependent. Initial results with recombinant proteins from kinase assays suggest that sorcin affects CaMKIIδ activity. In kinase experiments using a CaMKIIδ-selective peptide substrate, the presence of sorcin (10μM) significantly decreased CaMKIIδ-mediated phosphate incorporation (0.16±0.04 (control) vs 0.02±0.0002 (with sorcin) pmol phosphate incorporated/min/30ng CaMKIIδ, n=3, $p<0.05$).

Evidence is provided for an interaction between sorcin and CaMKIIδ. Sorcin appears to decrease CaMKIIδ activity. Under the assay conditions used, this could either reflect a direct modulation of CaMKIIδ or an ability to act as an alternative substrate. The significance of this interaction remains unclear however it may provide one route by which the CaMKIIδ/RyR2 interaction is modulated. Future experiments will examine the effects of sorcin overexpression on endogenous CaMKIIδ activity in isolated cardiac cells and more specifically, the effects on RyR2 associated kinase and function.

Currie S, Loughrey CM, Craig M-A & Smith GL (2004). *Biochem J* **377**, 357-366.

Lokuta AJ, Meyers MB, Sander PR, Fishman GI & Valdivia HH (1997). *J Biol Chem* **272**, 25333-25338.

Zhang T & Brown JH (2004). *Cardiovasc Res* **63**, 476-486.

This study is supported by the BHF.

Where applicable, the authors confirm that the experiments described here conform with the Physiological Society ethical requirements.

PC91

A model of canine cardiac ventricular wall electrophysiology

A.P. Benson[1], O.V. Aslanidi[2], H. Zhang[2] and A.V. Holden[1]

[1]Computational Biology Laboratory, Institute of Membrane and Systems Biology, University of Leeds, Leeds, UK and [2]Biological Physics Group, School of Physics and Astronomy, University of Manchester, Manchester, UK

Parameters in the Hund & Rudy (2004) canine epicardial (epi) cell electrophysiology model were altered to model differences in isolated endocardial (endo), midmyocardial (M) and epi cell current densities and kinetics, Ca^{2+} transients, and action potentials (APs), their duration (APD) and rate dependence.

Maximal conductances and fluxes were scaled with respect to epi values according to published experimental estimates: the late Na^+ current $I_{Na,L}$ by 1.15 and 1.7 for endo and M cells respectively; the transient outward K^+ current I_{to1} by 0.5 and 1.0; the slow delayed rectifier K^+ current I_{Ks} by 0.9 and 0.3; the Na^+-Ca^{2+} exchanger current I_{NaCa} by 0.4 and 0.5; and the Ca^{2+} uptake flux J_{up} by 0.6 and 0.7. The time course of reactivation of I_{to1} was modelled by altering the slow inactivation time constant to give values of 390, 456 and 264 ms at –80 mV in endo, M and epi cells, respectively. The activation time constant of the M cell rapid delayed rectifier K^+ current I_{Kr} was twice that in epi and endo cells at all membrane potentials.

Computed APs (Fig. 1A) quantitatively reproduce experimentally recorded APs and APD rate dependence (Fig. 1B). When the cell models were incorporated into a 15 mm virtual tissue strand composed of equal fractions of endo, M and epi tissue, electrotonic coupling reduces the transmural APD dispersion, prolongs the mean APD by ~20 ms, and smooths the gradient in APD (Fig. 1C). The conduction velocity of the depolarisation wavefront is approximately constant throughout the strand. The spatial distribution of repolarisation will be reflected in the ECG T wave.

The 3D ventricular wall is heterogeneous, rotationally anisotropic and orthotropic. However, the normal sinus rhythm ensures near-synchronous activation of the endocardial surface and so the excitation wavefront throughout the ventricles approximates a transmural plane wave. The 1D strand is therefore a computationally efficient model of the ventricular wall that can be used to study, for example, the transmural effects of anti-arrhythmic drugs (Aslanidi *et al.* 2004).

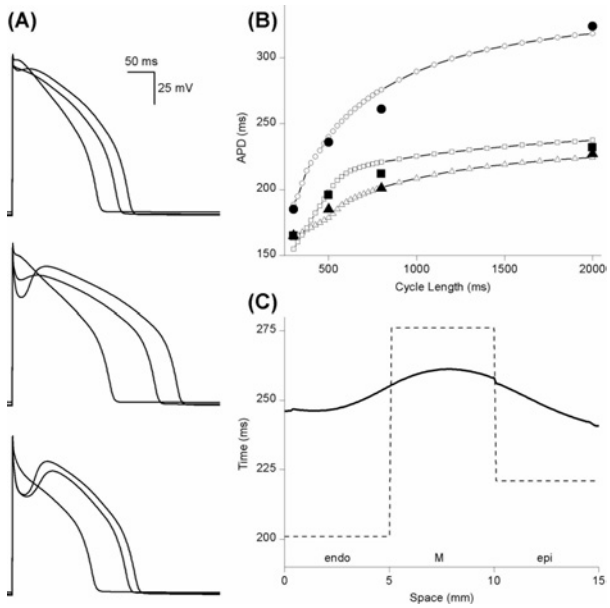

Figure 1. (A) APs in endo (top), M (middle) and epi (bottom) model cells at cycle lengths of 300, 800 and 2000 ms. (B) Model APD rate dependence (open symbols) and experimental data (filled symbols, from Liu *et al.*, 1993): triangles, endo; circles, M; squares, epi. (C) Transmural distribution of APD (solid line) in a 15 mm virtual tissue strand at a cycle length of 800 ms. Single cell steady-state values for a cycle length of 800 ms were used as initial conditions in the strand, which was then paced a further five times. Dashed line indicates APD distribution in uncoupled cells.

Aslanidi OV *et al.* (2004). *J Physiol* **561P**, PC23.

Hund TJ & Rudy Y (2004). *Circ* **110**, 3168-3174.

Liu DW *et al.* (1993). *Circ Res* **72**, 671-687.

This work was supported by the European Union through the Network of Excellence BioSim, contract No. LSHB-CT-2004-005137, and grants from the EPSRC and BBSRC. Alan Benson was supported by a MRC studentship.

Where applicable, the authors confirm that the experiments described here conform with the Physiological Society ethical requirements.

PC92

Quantifying the effects of Class III drugs on the canine ventricular tissue

O.V. Aslanidi[1], A.P. Benson[2], A.V. Holden[2] and H. Zhang[1]

[1]School of Physics and Astronomy, University of Manchester, Manchester, UK and [2]Institute of Membrane and Systems Biology, University of Leeds, Leeds, UK

Clinical trials show that Class III antiarrhythmic drugs (e.g., d-sotalol) have proarrhythmic side effects, and only amiodarone is relatively safe. At the cellular level, the drugs have different effects on the transmural dispersion of action potential duration (APD), which d-sotalol increases and amiodarone decreases. Our previous studies [1] suggested that such differences can account for the safety of amiodarone at the tissue level, as smaller APD

dispersion results in proportionally small vulnerable window (VW). In this study we quantify the effects of d-sotalol and amiodarone using detailed models, which are validated against respective experimental results for the canine ventricular tissue [2]. The Hund-Rudy [3] canine ventricular excitation model has been modified to reproduce the electrical restitution properties of endo-, M- and epicardial cells [4], as well as experimentally observed changes of these properties under the action of amiodarone and d-sotalol [2]. The resultant cell models were then incorporated into tissue models: a 1D strand model for transmural propagation, and a 3D wedge based on diffusion tensor MRI reconstruction of the canine ventricular architecture [5]. The standard S1-S2 protocol was used to measure vulnerability of the tissue defined as the time width of VW during which the S2 stimuli produced unidirectional conduction block. The models generate transmural APD dispersion patterns that are consistent with experiments on dogs treated with amiodarone and d-sotalol. The profile of VW is spatially heterogeneous, and correlates with the transmural APD dispersion (Fig. 1); VW is primarily wide in the epicardial region, where unidirectional block persists until the M-cells are fully repolarised. As d-sotalol increases and amiodarone decreases the APD dispersion, the VW in the latter region becomes proportionally larger or smaller (at maximum around 30 ms with d-sotalol, compared to 7 ms with amiodarone). S2 stimulation in the epicardial region of the 3D wedge within the VW results in sustained re-entry in case of d-sotalol; however, re-entry fails in control or with amiodarone. In conclusion, our results provide an electrophysiological explanation for the relative safety of amiodarone in comparison to d-sotalol, and quantify the vulnerability to re-entry in the canine ventricular tissues affected by the Class III drugs.

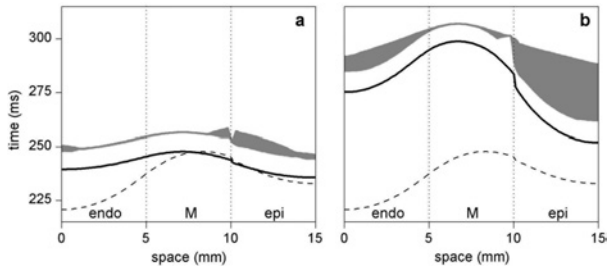

Figure 1. Transmural dispersion of APD_{90} (solid line) and spatio-temporal extent of the VW (grey area) in the 1D canine ventricular strand: (a) amiodarone and (b) d-sotalol; dispersion of APD_{90} in control is shown by dashed lines. The effect of d-sotalol is modelled by depressing I_{Kr} by 50% in endo-, by 70% in M- and by 20% in the epicardial cells; the effect of amiodarone is modelled by depressing I_{Ks} by 80% in endo- and by 30% in epicardial cells and depressing I_{Na1} by 80% in M-cells.

Aslanidi OV *et al.* (2004). *J Physiol* **561P**, PC23.

Sicouri S *et al.* (1997). *J Cardiovasc Electrophysiol* **8**, 1269-1279.

Hund TJ & Rudy Y (2004). *Circulation* **110**, 3168-74.

Benson AP *et al.* (2006). Proc Physiol Soc **3**.

Aslanidi OV *et al.* (2005). *J Physiol* **567P**, PC10.

This research was funded by the MRC and BBSRC.

Where applicable, the authors confirm that the experiments described here conform with the Physiological Society ethical requirements.

PC94

Rate and extracellular Ca^{2+}-dependent changes in contraction and the Ca^{2+} transient in ventricular myocytes treated with tumour necrosis factor-α and interleukin-1β

D.J. Duncan[1], P.M. Hopkins[2] and S.M. Harrison[1]

[1]Inst. Membrane and Systems Biology, University of Leeds, Leeds, UK and [2]Academic Unit of Anaesthesia, University of Leeds, Leeds, UK

Tumour necrosis factor-α (TNF-α) and interleukin-1β (IL-1β) serum levels are increased during the development of sepsis, reperfusion injury and heart failure and these agents either together or alone induce negative inotropic effects on the heart. The experiments described here were to assess the ability of isolated rat ventricular myocytes treated with these two cytokines, to regulate cytosolic Ca^{2+} and contraction during two inotropic interventions: (i) an increase in stimulation rate and (ii) elevation of extracellular Ca^{2+}. Treated cells were incubated (at 30 °C) for 3 hr in physiological salt solution supplemented with 0.05 ng/ml TNF-α and 2 ng/ml IL-1β and comparison made between control cells which were incubated in cytokine-free salt solution for the same duration. Cells were loaded with fura-2 to record cytoplasmic Ca^{2+} and cell shortening was recorded optically. Cells were field stimulated (1 or 3 Hz) at 30 °C and for treated cells, the superfusate included the same concentrations of cytokines used during incubation. Sarcoplasmic reticulum (SR) Ca^{2+} content was estimated from the peak of the Ca^{2+} transient evoked by rapid application of 20 mM caffeine. Data are presented as mean ± SEM.

In control cells (1 Hz stimulation, extracellular Ca^{2+} 1 mM) the Ca^{2+} transient and contraction were 0.24 ± 0.02 fluorescence ratio (Fr) units and 3.8 ± 0.4% of resting cell length, respectively (n = 24). In treated cells these parameters were reduced significantly ($P<0.05$, t test) to 0.16 ± 0.01 Fr units and 1.9 ± 0.4% of resting cell length, respectively, n = 24). Increasing stimulation rate to 3 Hz significantly increased ($P<0.001$, paired t test,) the magnitude of the Ca^{2+} transient, contraction and sarcoplasmic reticulum (SR) Ca^{2+} content in both control (n = 21-27) and treated cells (n = 21-29); however these three variables were all still significantly lower ($P<0.007$, t test) in treated than control cells. At 3 Hz, the time to peak and time for half relaxation of the Ca^{2+} transient and contraction were significantly accelerated compared to 1 Hz in both cell types ($P<0.05$, paired t test) but there were no additional cytokine-dependent changes in timecourse.

Elevating extracellular Ca^{2+} from 1 to 3 and 5 mM (at 1 Hz stimulation) increased Ca^{2+} transient and contraction amplitude in both control and treated cells ($P<0.05$, ANOVA, n = 16 & 21, 14 & 21 and 9 & 17 at 1, 3 and 5 Ca^{2+}, respectively); however, at both 3 and 5 mM Ca^{2+} we observed no significant cytokine-induced depression of contraction or the Ca^{2+} transient.

These data suggest that treated cells have a positive inotropic response to increasing stimulation rate but that contraction amplitude remained below that of control cells. However, elevation of extracellular Ca^{2+} abolished the inhibitory effects of TNF-α and IL-1β on the Ca^{2+} transient and contraction, illustrating a pivotal role for Ca^{2+} regulation in the negative inotropic effect of these cytokines.

Supported by The White Rose Consortium and The British Heart Foundation.

Where applicable, the authors confirm that the experiments described here conform with the Physiological Society ethical requirements.

PC95

Behaviour of blood pressure and heart rate immediately after termination of ventricular fibrillation

J.D. Schipke[1], F. Annika[1], W. Joachim[2], M. Kathrin[1] and E. Gams[2]

[1]Research Group Experimental Surgery, University Hospital, Duesseldorf, Germany and [2]Dept. of Thoracic and Cardiovascular Surgery, University Hospital, Duesseldorf, Germany

Sudden cardiac death (SCD) from any cause claims 300,000–400,000 lives a year in the US. Implantable cardioverter/defibrillators (ICDs) can detect ventricular fibrillation (VF) and terminate it. For determining the optimal defibrillation threshold, ventricular fibrillation is repetitively induced intraoperatively and terminated using DC shocks of different energy. Depending on the protocol employed, several fibrillation/defibrillation sequences are mandatory before the final implantation of an ICD, thus providing an elegant model to study how LV peak pressure and RR interval develop after the termination of VF in anaesthetized patients.

The 34 patients (6 females; 18%) averaged 59±10 years (from 33 to 79 years). The anaesthetic regimen was standardized for all patients. Anaesthesia was maintained with 1.5% enflurane. The ventilation was controlled; the end-expiratory pressure was set to zero. Left ventricular (LV) pressure was assessed using a microtip-catheter. ECG leads I, III und V_5 were recorded. In all patients, VF was induced with a fibrillator. After conclusion of the defibrillation threshold testing and implantation of the cardioverter/defibrillator, the functionality of the implanted device was tested by a final induction of VF and its subsequent termination by the ICD (the device test). LV peak pressure after a total of 157 VF terminations was used to derive an exponential function:

$LVP(t) = A \times (-\exp(-t/\tau LVP)) + B$,

with A, factor to determine the starting pressure [mmHg] at t = 0 s; τLVP, constant of LV pressure increase [beats]; and B, non-zero asymptote [mmHg]. The decrease in the RR-interval (RRI) was described with the exponential equation:

$RRI(t) = C \times \exp(-t/\tau RRI) + D$,

with C, factor to determine the starting RRI [s] at t = 0 s; τRRI, constant of RRI increase [beats]; and D, non-zero asymptote [s]. Data are means±SD.

The exponential equation described the time-dependent peak LVPs and the RRIs very closely (r2 was 0.96±0.08 and 0.62±0.27 respectively). The LVP increased with a constant of 8±3 beats. The RRI decreased clearly quicker with a constant of 2±1 beats (t test, $P<0.05$).

After termination of VF, peak LVP will plateau after about 40 beats whereas the heart rate will already plateau after about 10 beats, i.e. after 5 times τ. Thus, the heart 'finds' a steady state rhythm quicker than the individual peak systolic pressure does.

Where applicable, the authors confirm that the experiments described here conform with the Physiological Society ethical requirements.

PC96

Activity-dependent changes of $[Ca^{2+}]$ in the transverse-axial tubular system reduce SR $[Ca^{2+}]$ content and $[Ca^{2+}]$ transient amplitude in rat and guinea pig cardiac ventricular myocytes: a simulation study

M. Pásek[1], J. Šimurda[2], C.H. Orchard[3] and G. Christé[4]

[1]Institute of Thermomechanics, Czech Academy of Science, Brno, Czech Republic, [2]Department of Physiology, Masaryk University Brno, Brno, Czech Republic, [3]Department of Physiology, University of Bristol, Bristol, UK and [4]INSERM, Lyon, France

To explore the physiological consequences of ion concentration changes in the transverse-axial tubular system (TATS) of rat and guinea-pig cardiac ventricular myocytes we have developed mathematical models of their electrical activity that include a quantitative description of the TATS (e.g. Pásek et al., 2003). The geometrical characteristics of the TATS, and the characteristics of ion transporters and their distribution between the surface and tubular membranes, were modelled using available experimental data from each species.

In both models, transient depletion of tubular Ca^{2+} occurred during each action potential and decreased intracellular Ca^{2+} load and consequently systolic Ca^{2+} transient amplitude. However, the magnitude of this effect and its frequency dependence was different in the two species. In the rat model, the maximal depletion of tubular Ca^{2+} during a single period, at a stimulation rate of 1 Hz, was 7 %. With increasing stimulation frequency, tubular Ca^{2+} depletion increased, reaching 13.1 % at 5 Hz. This depletion induced a cumulative beat-to-beat decrease in SR Ca^{2+} content that resulted in ~3 % decrease of steady-state Ca^{2+} transient amplitude at 1 Hz and ~20 % decrease at 5 Hz. In the guinea pig model, the maximal depletion of tubular Ca^{2+} was 13.8 % at 1 Hz, which decreased with stimulation frequency, to 6.5 % at 5 Hz. The reduction of Ca^{2+} transient amplitude was lower than in rat: 3 % at 1 Hz and 1.2 % at 5 Hz.

These differences arise because: (i) the fraction of I_{Ca} in the TATS, which is responsible for tubular Ca^{2+} depletion, is lower in the guinea-pig (64 %, Shepherd & McDonough, 1998) than in the rat (87 %, Brette & Orchard, 2003); (ii) the sensitivity of I_{Ca} to the changes of membrane potential induced by tubular Ca^{2+} depletion is lower in guinea pig; (iii) unlike the rat model, the magnitude of I_{Ca} decreases with stimulation frequency in the guinea pig model; (iv) ion diffusion between the tubular lumen and external space is significantly faster in the guinea pig model (τ_{Ca}= 240 ms; Shepherd and McDonough, 1998) than in the rat model (τ_{Ca}= 500 ms; Yao et al., 1997); however Blatter & Niggli (1998), suggest that τ_{Ca} may be > 1000 ms in guinea pig, which would increase Ca^{2+} depletion in guinea pig TATS. These data suggest that changes of ion concentrations occur in the TATS lumen and modulate cell function.

Blatter LA & Niggli E (1998). *Cell Calcium* **23**, 269-279.

Brette F & Orchard C (2003). *Circ Res* **92**, 1182-1192.

Pásek M *et al.* (2003). *Gen Physiol Biophys* **22**, 355-368.

Shepherd N & McDonough HB (1998). *Am J Physiol* **275**, H852-H860.

Yao A *et al.* (1997). *Cell Calcium* **22**, 431-438.

Supported by the projects AV0Z 20760514 and MSM 0021622402.

Where applicable, the authors confirm that the experiments described here conform with the Physiological Society ethical requirements.

PC97

Demonstration of functional dipeptide transport in isolated cardiomyocytes

H. Lin and N. King

Clinical Science «Xtags error: Unexpected end of line»

Amino acids are used in the heart for protein synthesis, energy production and signal transduction (1). This is facilitated by amino acid transport across the cardiac sarcolemma. In the kidney and small intestine, the proton coupled transporters, PEPT1 (gene name SLC15A1) and PEPT2 (gene name SLC15A2) provide an extremely efficient mechanism for the transport of bulk quantities of amino acids in the form of small peptides (2). PEPT1 and PEPT2 are also important pharmacologically since they transport peptidomimetic compounds such as angiotensin converting enzyme (ACE) inhibitors and β-lactam antibiotics (2). The aim of this investigation was to investigate whether these transporters are expressed and active in isolated ventricular cardiomyocytes.

Ventricular cardiomyocytes were isolated from adult male guinea-pigs by enzyme and mechanical dispersion techniques as described previously (3). The oil filtration centrifuge stop technique used to measure the uptake of 0-3mM L-glycyl-L-[^{14}C]sarcosine (gly-sar) into the cardiomyocytes has also been described (4). The only modification to the published method (4) was the use of Mes/Tris instead of Hepes/Tris to prepare solutions with pH ≤ 6.5. Reverse transcription polymerase chain reaction (5) was used to investigate the expression of PEPT1 and PEPT2 in the cardiomyocytes. Results are expressed in terms of intracellular space (i.e. as pmol/μl intracellular space as described in (4)) and are means ± S.E.M. of 4 or 5 experiments.

The uptake of 200μM gly-sar at 30 s after dipeptide addition was strongly dependent on external pH with transport greatest at pH 5.75 (217.8 ± 15.8 pmol/μl), and least at pH 8.0 (72.1 ± 13.4 pmol/μl, $p<0.01$, t test). At pH 6.0, the initial rate of gly-sar uptake obeyed Michaelis-Menten kinetics with a K_m of 495.5 ± 69.6μM and a V_{max} of 1470.5 ± 69.6 pmol/μl/min. The control initial rate of gly-sar uptake at pH 6.0 of 343.8 ± 7.5 pmol/μl/min, was significantly reduced by the addition of 10mM of the ACE inhibitor, enalapril (92.2 ± 31.2 pmol/μl/min); or of the β-lactam antibiotics, cefadroxil (82.9 ± 32.7 pmol/μl/min), cephaloridine (116.7 ± 11.6 pmol/μl/min) or ampicillin (103.5 ± 12.2 pmol/μl/min); or of various L-amino acid containing di- or tri-peptides (all comparisons, $p<0.01$, ANOVA with a Dunnett post test). In contrast, 10mM of the constituent amino acids, glycine (336.2 ± 11.1 pmol/μl/min) or sarcosine (339.4 ± 18.2 pmol/μl/min) or of the D-amino acid containing dipeptide D-ala-D-ala (367.2 ± 25 pmol/μl/min) did not significantly alter the control uptake. PEPT2 specific primers recognised mRNA of the appropriate size in kidney (positive control) and cardiomyocytes, whilst PEPT1 was expressed in kidney but not cardiomyocytes. These results provide the first evidence supporting the presence of a functional dipeptide transporter in isolated cardiomyocytes.

Pisarenko OI (1996). *Clin Exptl Pharmacol Physiol* **23**, 627-633.

Daniel H & Kottra G (2004). *Pflügers Archiv* **447**, 610-618.

Rodrigo GC & Chapman RA (1990). *Exp Physiol* **75**, 839-842.

King N & Suleiman M-S (2001). *Mol Cell Biochem* **221**, 99-108.

King N. *et al.* (2004). *J Physiol* **556**, 849-858.

Supported by the BHF.

Where applicable, the authors confirm that the experiments described here conform with the Physiological Society ethical requirements.

PC98

Effect of homocysteine on the isolated and perfused rat heart during ischaemia-reperfusion

D. Shackebaei[1], N. King[2] and M. Suleiman[2]

[1]*Medical Biology Research Centre, Kermanshah University of Medical Sciences, Kirmanshah, Iran and* [2]*Clinical Science* «Xtags error: Unexpected end of line»

A raised plasma level of homocysteine or hyperhomocysteinaemia (HHcy) is a strong independent risk factor for atherosclerotic and/or thrombotic disease (1,2). It is not currently known whether HHcy is a cause or a symptom of these conditions; nonetheless it has been reported that homocysteine may be pro-inflammatory, or a stimulator of either oxidative or endoplasmic reticulum stress (1,2). To date the majority of studies have concentrated upon vascular endothelial cells, smooth muscle cells or monocytes (1,2) with relatively little known about the whole heart under normal and pathological conditions. Therefore the aim of this study was to investigate the effects of homocysteine upon the function of the isolated and perfused heart before, during and after exposure to global ischaemia.

Hearts from male adult Wistar rats were perfused with oxygenated Krebs at 37°C in the Langendorff constant pressure mode as previously described (3). After an initial equilibration period (at least 20 min), hearts (n = 12-13 per group) were exposed to 45 min global normothermic ischaemia followed by 30 min reperfusion. Throughout the experiment cardiac function was monitored via a thin-walled fluid filled balloon inserted into the left ventricle (3). Where used, 0.5mM homocysteine was constantly present from 30 min before ischaemia until 10 min into reperfusion when it was washed out. Results are presented as means ± s.e.m.

Under normal conditions pre-ischaemia, perfusion with 0.5mM homocysteine caused a significant increase in coronary flow compared to control without homocysteine (16.6 ± 0.5 vs. 13.9 ± 0.9ml/min; $p < 0.02$, t test). Thereafter, the homocysteine perfused hearts showed a poorer functional recovery. At 30 min reperfusion the rate pressure product (RPP, heart rate in beats per minute (bpm) x left ventricular developed pressure in mmHg x 10^3) of control hearts was 9.3 ± 0.8 compared to 6.9 ± 0.8 in the with homocysteine group ($p<0.05$, t test). There were no significant differences in the RPP prior to ischaemia (control, 22.0 ± 1.3 vs. with homocysteine, 21.2 ± 1.0 bpm x mmHg x 10^3) or in the time to ischaemic contracture between the two groups (control, 16.8 ± 1.2 vs. with homocysteine, 19.2 ± 1.1 min). These results suggest that homocysteine cause changes to the coro-

nary blood flow and vessels, which increase susceptibility to a subsequent ischaemic insult.

de Koning ABL *et al.* (2003). *Clin Biochem* **36**, 431-441.

Refsum H & Nygård O (1998). *Annu Rev Med* **49**, 31-62.

Schackebaei *et al.* (2005). *Mol Cell Biochem* **277**, 27-31.

Supported by the BHF.

Where applicable, the authors confirm that the experiments described here conform with the Physiological Society ethical requirements.

PC99

Evaluation of cardiac cell membrane capacitance from the current response to a small pulse. Compared reliability of numerical integration versus fitting an exponential decay

G. Christe[1], Y. Zhang[1], E. Ricci[2], C. Chouabe[2] and R. Bonvallet[2]

[1]INSERM, Lyon, France and [2]CNRS UMR 5123, Université Lyon 1, Villeurbanne, France

The measurement of the membrane capacitance (C_m) of single cardiac cells is required for normalization of ionic current densities allowing comparison across cell types and species. It is also needed for estimating the fraction of cell membrane located in transverse-axial tubules in cardiac cells and as part of the characterization of cellular hypertrophy. While sophisticated automated techniques are available in recently developed patch-clamp amplifiers, a common approach is still off-line analysis of the current in response to a small voltage-clamp pulse applied from the resting voltage. Experiments were carried out on single ventricular myocytes isolated from male Sprague-Dawley rats under whole-cell voltage clamp.

We analysed the biases and errors for two most commonly used methods of C_m evaluation: (a) the method based on least-squares adjustment of the current decay by a single exponential function (with time constant τ) plus offset and (b) the numerical integration of the decaying part of the current.

In method b three possible conceptual biases on C_m evaluation are considered: (1) integration is not feasible before a finite time t_1 from the start of the charging pulse; (2) neglecting that the voltage across the fully charged C_m is the command voltage multiplied by a factor $R_m/(R_s+R_m)$, that involves finite membrane resistance R_m and non-zero series resistance R_s; (3) a fraction of the charging current cannot be directly integrated. Each of these biases cause underestimation of C_m.

A simple method is proposed to recalculate the complete integral from time zero of the voltage clamp pulse. Corrective factors are derived that allow a posteriori compensation of each of the three biases on Cmb estimated by method b, i.e.: factor 1 = $[\exp(t_1/\tau)]$ for bias (1), and a identical factor 2 = $[(R_s+R_m)/R_m]$ for each of biases (2) and (3). The global correction factor $[(\exp(t_1/\tau))*((R_s+R_m)/R_m)^2]$ compensates for all three biases.

The influence of these biases was studied on capacitance current responses from 923 rat ventricular myocytes to a 10 mV depolarising pulse from -80 mV. In a subset of 520 cells with intact K^+ currents, individual estimates of C_m from both methods are compared in Fig. 1. The relative difference $(C_{ma} - C_{mb})/C_{ma}$ was –29 ± 9% in 'nC', -19 ± 13% in 'C1', -7.6 ± 8.6% in 'C23', and +4.6 ± 7.8% in 'C123'. In the remaining 403 cells recorded with blocked K^+ currents (not illustrated), these relative differences were, respectively: –10.2 ± 5.0% in 'nC', 1.0 ± 4.0% in 'C1', -7.8 ± 5.6% in 'C23', and +3.7 ± 3.6% in 'C123'. Thus, application of the global correction factor $(\exp(t_1/\tau))*((R_s+R_m)/R_m)^2$ compensates for all three biases in method b and yields final C_m values that closely match those from method a.

Using a Monte-Carlo approach, a 10 pA rms noise was added to a synthetic capacitance record computed assuming C_m=300 pF, R_s=2 MΩ and R_m=20 MΩ. This was repeated 5000 times, the mean ± SD of estimates of C_m, R_s and R_m were, respectively, 300 ± 0.34, 2 ± 0.002 and 20 ± 0.09 for method a, and 300.1 ± 5.5, 2 ± 0.09 and 20 ± 0.14 for method b.

It is concluded that, provided biases are compensated for, with realistic noise levels, and even when resting membrane conductance is large, both methods give equally reliable estimates of C_m.

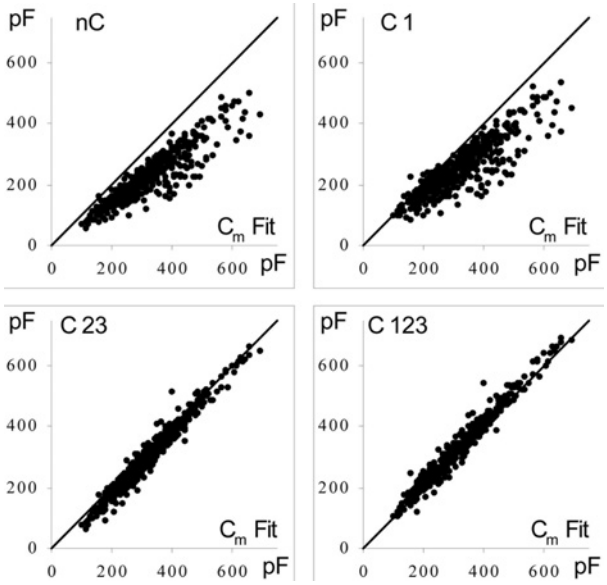

Figure 1. Capacitance charging current responses from 520 cells without blockers of K^+ currents were analysed. C_m values from method b (ordinates) were plotted versus those from method a (abscissas). C_m values from method b were uncorrected in panel 'nC', corrected for bias (1) in panel 'C1', for both of biases (2) and (3) in panel 'C23' and for all three biases in panel 'C123'. The solid line is the identity line.

This work was supported by a research grant to G.C. from the 'Fédération des Maladies Orphelines', Paris, France. Y.Z. is a student of the 'Approches Mathématiques et Informatique du Vivant' (aMIV) Université Lyon 1, Villeurbanne, France.

Where applicable, the authors confirm that the experiments described here conform with the Physiological Society ethical requirements.

PC100

Clemastine, a conventional antihistamine, is a high potency inhibitor of the HERG K^+ channel

J.M. Ridley[1], J.T. Milnes[2], J.C. Hancox[1] and H.J. Witchel[1]

[1]Physiology, University of Bristol, Bristol, UK and [2]Xention Discovery Ltd., Cambridge, UK

HERG (*human ether-à-go-go-related gene*) encodes the α-subunit of channels carrying the cardiac rapid delayed rectifier K^+

current (I_{Kr}), which is a major determinant of the duration of ventricular action potentials and of the QT interval. This study investigated the effects on HERG channel current (I_{HERG}) of clemastine, a 'conventional' antihistamine that has been associated with delayed ventricular repolarization in vitro [1,2], but for which no adverse effects on human QT interval have been reported. Whole-cell patch-clamp measurements of I_{HERG} were made at 37°C from human embryonic kidney (HEK 293) cells stably expressing HERG channels [3]; the extracellular solution was normal Tyrode solution, and the pipette solution was a physiological K-based solution. I_{HERG} tails at -40 mV following two-second depolarizing pulses to +20 mV were inhibited by clemastine with an IC_{50} value of 12 nM; this drug concentration also inhibited peak I_{HERG} by 41.1 ± 1.2% (mean ± SEM) when elicited during a voltage-clamp command of a digitised rabbit ventricular action potential. Clemastine produced a reversible ~ -5 mV shift in the I_{HERG} steady-state voltage-dependent activation curve, but voltage dependence of inactivation was unaffected. Development of I_{HERG} inhibition by clemastine showed strong time-dependence. The S6 point mutation Y652A greatly attenuated the inhibitory effect of 120 nM (10X IC_{50}) clemastine from 89.4 ± 2.5% block (WT) to 19.3 ± 4.3% (Y652A-HERG), as did the mutation F656A, which reduced inhibition from 84.5 ± 1.4% block (WT) to 9.0 ± 6.1% block (F656A-HERG), all when using protocols and conditions previously described for these mutant channels [3] (n = 5 or 6 for all, $P < 0.001$). We conclude that clemastine is a high potency inhibitor of the HERG K^+ channel, exhibiting characteristics of a preferential open/activated channel blocker and interacting with a high affinity drug-binding site in the HERG channel pore cavity. The disparity between clemastine's potent I_{HERG} inhibition and a lack of QT-prolongation in normal clinical use underscores the need to interpret HERG IC_{50} data for novel compounds in the context of information from other safety assays.

Ki I, Inui A & Ito T (1996). Arch Int Pharmacodyn Ther 331, 59-73.

Wang WX, Ebert SN, Liu XK, Chen YW, Drici MD & Woosley RL (1998). J Cardiovasc Pharmacol 32, 123-128.

Milnes JT, Crociani O, Arcangeli A, Hancox JC & Witchel HJ (2003). Brit J Pharmacol 139, 887-898.

The authors thank Professor J Vann Jones and the Charitable Trusts for the United Bristol Hospitals for support of J.M.R. Support from the British Heart Foundation and technical assistance from Mrs Lesley Arberry are also gratefully acknowledged.

Where applicable, the authors confirm that the experiments described here conform with the Physiological Society ethical requirements.

PC101

Guinea pig isolated cardiomyocyte elastance as a universal descriptor of contractile properties in isometric and isotonic contractions

G. Iribe[1], M. Helmes[2] and P. Kohl[1]

[1]University of Oxford, Oxford, UK and [2]IonOptix Europe, Wageningen, Netherlands

To investigate contractile profiles of Guinea pig single isolated cardiac myocytes in isometric and isotonic contractions, we used a pair of compliant, computer-controlled and piezo-translator (PZT) positioned carbon fibers (CF), attached glue-free to opposite cell-ends, and an optical force-length (FL) feedback system. Guinea pigs hearts were quickly excised post mortem, and cells were enzymatically isolated, using established Langendorff perfusion-based protocols. Once CF attachment was established, cells were lifted off the coverslip and paced at 2 Hz in normal Tyrode solution (37°C). CF-tip distance was monitored in real time, and passive/active forces were calculated from CF bending. Isometric and isotonic contractions were imposed by applying appropriate PZT commands, both at moderate (initial sarcomere length, SL, ~1.94 μm) and high (initial SL ~2.05 μm) preloads. Contractile properties, both during isometric and isotonic contractions, were quantified via analysis of instantaneous elastance curves, which describe the time-course of changes in the slope of a line connecting the instantaneous position in force-length space with the intersection point of end-diastolic and end-systolic force-length relations (minimum point).

Altering preload did not affect time to peak elastance, neither in isometric nor isotonic conditions, but led to a significant slowing of relaxation at high afterload (i.e. during isometric contractions). Increasing afterload, i.e. switiching from isotonic to isometric contraction at a given preload, increased time to peak elastance (see Table 1 and Fig. 1). These results are consistent with previous findings on the shortening-induced decrease, and stretch-induced increase, in Ca^{2+} affinity of myofilaments [1]. Thus, combining the CF technique with dynamic FL control enables one to trace elastance curves, instead of either force or shortening, which aids comparison of the contractile profiles via a single parameter (elastance) for various loading conditions, including isometric and isotonic (where the traditional approach is limited).

Table 1. Pre- and afterload-dependent changes in time to peak elastance and relaxation in elastance curve

Preload condition	Low		High	
End-diastolic SL (μm)	1.939 ± 0.008		2.050 ± 0.025†	
Afterload condition	Low (Isotonic)	High (Isometric)	Low (Isotonic)	High (Isometric)
Time to peak elastance (ms)	60.26 ± 2.9	53.5 ± 1.8*	61.9 ± 1.6	56.4 ± 1.5*
Relaxation time constant (ms)	9.74 ± 0.89	15.83 ± 1.28*	9.73 ± 1.35	22.97 ± 1.24*†

Mean ± SEM (n = 13). *$p < 0.05$ vs Isotonic; $p < 0.05$ vs low preload.

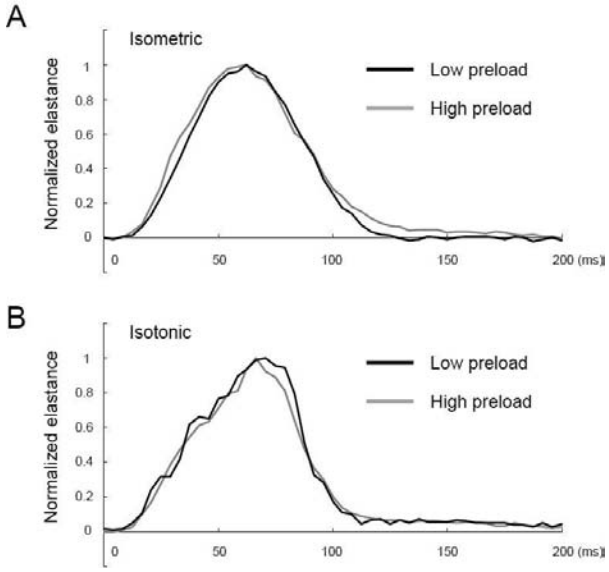

Figure 1. Pre- and afterload-dependent morphological changes in elastance curve.

Allen, D. G. & Kurihara, S. 1982 The effects of muscle length on intracellular calcium transients in mammalian cardiac muscle. J Physiol 327, 79-94.

Where applicable, the authors confirm that the experiments described here conform with the Physiological Society ethical requirements.

PC102

Electromechanical properties of isolated myocardium from patients with hypertrophic obstructive cardiomyopathy (HOCM)

R. Gray[1], P. Dhillon[2], N. Peters[2], W. McKenna[3] and C. Fry[1]

[1]Institute of Urology, University College London, London, UK, [2]Cellular Electrophysiology, St Mary's Hospital, London, UK and [3]The Heart Hospital, London, UK

Hypertrophic cardiomyopathy is associated with increased risk of arrhythmias and heart failure, and sudden cardiac death especially in younger people (McKenna et al. 2002). The hypertrophy is often asymmetric involving the septum and, in a proportion of patients there is left ventricular outflow obstruction. The histological hallmark is myocyte disarray and fibrosis. The cellular basis of the functional abnormalities is unclear and there is no extensive description of the electromechanical properties of human myocardium from such patients.

Myocardial strips (≤1 mm diameter) were prepared from surgically excised, septal myocardium from 14 symptomatic patients with HOCM, and normal systolic function at rest. Samples were also snap-frozen in liquid N_2 for estimation by Western blotting of connexin43 (Cx43) protein (Peters et al. 1997). Electromechanical properties, including action potential morphology and conduction, isometric twitch characteristics and impedance properties were measured as described previously (Cooklin et al. 1997; Botchway et al. 2003). Data are mean±SD and compared where possible to a previous study (McIntyre & Fry, 1997) that used samples from patients with mitral stenosis (MS) and normal ventricular function. Differences between groups were tested with Student's t test and the null hypothesis rejected at $p<0.05$.

All samples had a negative force-frequency function; the tension ratio at 1.6 and 0.8 Hz stimulation was 0.84±0.09 and significantly less than the MS group (1.30±0.22). Time to peak tension generation was not significantly different in the two groups (262±31, 260±27 ms; HOCM vs MS), but time to relaxation was significantly longer in the HOCM group (402±43 vs 307±20 ms). Isoprenaline increased significantly tension generated at 1 Hz by 243±53% at 3 μM, with an EC_{50} of 0.64±0.22 μM (n=5). Action potential duration (95% repolarisation) at 1Hz stimulation was significantly longer in the HOCM group (455±84 vs 342±11 ms), and often displayed early after-depolarisations at lower stimulation frequencies. Conduction velocity was also significantly less in HOCM samples (51.3±4.6 [n=6] vs 59.9±6.1 cm s^{-1} (n=9)). A negative association (r=0.88, n=7) was observed between the amount of Cx43 protein (normalised to f-actin) and the intracellular resisitvity measured by impedance network analysis.

We show that with myocardium from patients HOCM, action potential and twitch durations are both prolonged and that action potential conduction is also impaired. We propose that slowed conduction is due to reduced Cx43, and hence increased intracellular resistivity. These observations may explain why patients with HOCM tolerate tachycardia poorly and are prone to malignant arrhythmias.

McKenna WJ, Firoozi S & Sharma S (2002). Card Electrophysiol Rev 6, 26-31.

Peters NS, Coromilas J, Severs NJ & Wit AL (1997). Circulation 95, 988-996.

Cooklin M, Wallis WR, Sheridan DJ & Fry CH (1997). Circ Res 80, 765-771.

Botchway AN, Turner MA, Sheridan DJ, Flores NA & Fry CH (2003). Cardiovasc Res 60, 510-517.

McIntyre H & Fry CH (1997). J Cardiovasc Electrophysiol 8, 887-894.

Supported by the British Heart Foundation.

Where applicable, the authors confirm that the experiments described here conform with the Physiological Society ethical requirements.